joge manuscript No.
(will be inserted by the editor)

Distribution and mitigation of higher order ionospheric effects on precise GNSS processing

Manuel Hernández-Pajares · Àngela Aragón-Ángel · Pascale Defraigne · Nicolas Bergeot · Roberto Prieto-Cerdeira · Jaume Sanz · Alberto García-Rigo

Received: date / Accepted: date

M. Hernández-Pajares, A. Aragón-Àngel, J. Sanz, A. García-Rigo

Res. group of Astronomy and Geomatics (gAGE)

Technical University of Catalonia (UPC)

Mod. C3 Campus Nord UPC

Jordi Girona 1-3, 08034 Barcelona, Spain

E-mail: manuel@ma4.upc.edu

P. Defraigne, N. Bergeot

Royal Observatory of Belgium (ROB)

Solar Terrestrial Center of Excellence (STCE)

Avenue Circulaire, 3

Brussels, Belgium

E-mail: pascale.defraigne@oma.be

R. Prieto-Cerdeira

European Space Agency (ESA)

Keplerlaan 1

Noordwijk, The Netherlans

Abstract Higher order ionospheric effects (I2+) are one of the main limiting factors in very precise GNSS processing, for applications where millimeter accuracy is demanded. This manuscript proposes a comprehensive study of the I2+ effects in range and in GNSS precise products such as receiver position and clock, tropospheric delay, geocenter offset, GNSS satellite position and clocks. All the relevant higher order contributions are considered: second and third order, geometric bending and dSTEC bending (i.e. the difference between the STEC for straight and bent paths). Using a realistic simulation with representative Solar Maximum conditions on GPS signals, both the effects and mitigation errors are analyzed. The usage of the combination of multifrequency L-band observations to cancel out the main effect, i.e. the second order ionospheric term, has to be rejected due to its increased noise level, seen in both analysis of actual data and theoretical considerations. The results of the study show that the main two effects in range come from the second order ionospheric term and the dSTEC bending: daily average values of 5 mm are obtained for second order term and up to 2 mm error for dSTEC bending (with peak values up to +20 mm and up to +14 mm respectively at south azimuth and 10 deg. of elevation). Their combined impact on the precise GNSS satellite products affects the satellite Z-coordinates (up to +1 cm) and satellite clocks (more than +/- 20 ps). Other precise products are affected at the millimeter level (+/- 2 mm in the case of the receiver position, up to about +/- 15 ps in the receiver clock and up to more than 1 mm in the non-hydrostatic tropospheric vertical delay). After correction, with approximate affordable models, the impact on all the precise GNSS products is reduced below 5 mm. We finally quantify the corresponding impact on a Precise Point Positioning (PPP) processing, after

E-mail: Roberto.Prieto.Cerdeira@esa.int

applying consistently the precise products (satellite orbits and clocks) obtained under correction of higher order ionospheric effects: the remaining effect is shown to be lower than the current uncertainties of the PPP solutions.

Keywords Ionospheric higher order terms · Precise GNSS processing

1 Introduction

The first order ionospheric term ($I1$) is the main contributor to the ionospheric delay of GNSS observations, compared with the less than 0.1% corresponding to the higher order ionospheric terms (see for instance Brunner & Gu 1991, Bassiri & Hajj 1993, Kedar et al. 2003).

It is well known that I1 is proportional to the number of free electrons encountered in a cylinder with a base of unity area around GNSS transmitter-to-receiver path (also called Slant Total Electron Content, STEC), and inversely proportional to the squared carrier frequency f (see for instance Hernández-Pajares et al. 2011). Then it can be fully removed (under the assumption of straight line propagation) when combining simultaneous measurements at two frequencies f_1 and f_2. In this way the so called *ionospheric-free* combinations of carrier phase ($L_c \equiv L_3 \equiv \frac{f_1^2 L_1^2 - f_2^2 L_2}{f_1^2 - f_2^2}$) and code ($P_c \equiv P_3 \equiv \frac{f_1^2 P_1^2 - f_2^2 P_2}{f_1^2 - f_2^2}$) only contain the higher order ionospheric signature.

However, because of the increasing accuracy demand in some GNSS applications, and in general in Space Geodesy, the study of the impact of the higher ionospheric terms –up to few centimeters in range- has become relevant (see, for instance, King et al. 2010).

In this context, the main goal of this work is to show the overall impact of each higher order ionospheric term in both: the precise combination of GNSS observations

Lc, and in each precise GNSS product. This is done after showing the lack of usefulness of three-frequency measurements combination as a practical solution to remove the second order ionospheric term I_2.

The manuscript is divided into seven main sections. After this introduction, a summary of the higher order ionospheric effects is given. In section 3, we show with actual data the unfeasibility to remove as well the second order ionospheric term, by combining simultaneous transmitter-receiver GNSS L-band measurements in three frequencies. Section 4 describes the simulation of I2+ terms on the GNSS signal range, under nominal solar maximum conditions provided by the International Reference Ionosphere model (IRI; see, for instance Bilitza et al. 2011). In Section 5, we quantify the impact of I2+ on precise GNSS products and the remaining error when the I2+ terms are corrected using simplified affordable models. In the next section, the impact on GNSS precise products and user positioning is summarized. The last section sum up the conclusions and proposes several recommendations.

2 Summary of higher order ionospheric terms

For a given carrier frequency f, the GNSS measurement with the highest precision is the carrier phase L_f. It can be expressed in terms of (1) a non-dispersive term $\rho^\star$ (including the geometric distance, receiver and transmitter clock errors, relativity term and tropospheric delay), (2) its ambiguity B_f (the unknown initial pseudorange at phase locking time), (3) the wind-up ϕ (phase rotation term) and (4) the first, second and third order ionospheric terms. For the latest terms we can consider a straight line propagation approximation ($I_{f,1}$, $I_{f,2}$ and $I_{f,3}$, respectively), as well as a geometric (i.e. excess path) bending term ($I_{f,g}$) and a difference of STEC between the actual

slightly bent path versus the straight line propagation (dSTEC term $I_{f,d}$):

$$L_f = \rho^\star + B_f + \frac{c}{f}\phi + I_{f,1} + I_{f,2} + I_{f,3} + I_{f,g} + I_{f,d} \quad (1)$$

The most relevant information on all the considered ionospheric terms is summarized in Table 1: their exact expressions are provided (third column) as well as every approximation considered in this paper (fourth column). Note that the third order ionospheric term has been split into two contributions ($I_{f,3} = I_{f,3,M} + I_{f,3,s}$) in terms of the magnitude, the main one ($I_{f,3,M}$) and the smaller one ($I_{f,3,s}$). In detail: $\int_S^R X dl$ represents the straight line path integral of expression X (higher order terms listed in Table 1) from satellite to receiver; I_f and I_c are the corresponding terms for frequency f and for the first-order ionospheric free combination, respectively; f_1 and f_2 are the frequencies of L_1 and L_2 measurements; N_e is the electron density and N_m is its corresponding maximum; B is the geomagnetic field modulus; θ is the angle between the GNSS signal propagation direction and the geomagnetic field; r is the geocentric distance and $a = r\cos E$ is the GNSS ray impact parameter being E the elevation; M is the mapping function, V is the vertical total electron content (VTEC); S is the STEC; and finally, $H_{F2} = \frac{V}{\sqrt{2\pi}eN_m}$ and $h_{m,F2}$ are the $F2$-layer scale height and the electron density maximum, respectively. The shape parameter $\eta \equiv N_e/(N_m \cdot VTEC)$ is taken as $\eta = 0.66$ (corresponding to assuming the following Chapman model for the electron density distribution: $N_e = N_m \exp(k[1 - z - \exp(-z)])$, where $k = 1/2$). In [*] of Table 1 (see Hoque and Jakowski, 2008), and among the elevation E which is expressed in radians with $\beta = 2.13$, the following NON-SI units are used: the geometric bending is expressed in millimetres while STEC is expressed in TECU (1 TECU= $10^{16} m^{-2}$), the scale height H_{F2} and the peak ionization height H_{F2} in kilometers; and finally the frequency f is given in GHz, when used in the $1/f^4$ factor. On the other hand, in [**]

(see Jakowski et al. 1994) the following NON-SI units are considered: the geometric bending is as well expressed in millimetres and the STEC in TECU, but the frequency f is given in MHz. In [***] NON-SI units are taken as well (see Hoque and Jakowski, 2008): where the elevation is in radians with $\gamma = 2.1844$, H_{F2} and hm_{F2} are in kilometers, f is in Hz and STEC and resulting dSTEC bending are in m^{-2} (its effect is then applied as $-40.309 \cdot$dSTEC-bending$/f^2$).

3 Unfeasibility to remove the second order ionospheric term with three-frequency L-band measurements combinations

Several authors have pointed out the possibility to cancel the second order ionospheric term $I_{f,2}$ in Equation 1, similarly and simultaneously as it is done with the first order term $I_{f,1}$, by combining three simultaneous measurements (instead of two) of the GNSS carrier phases $L_{f_1}, L_{f_2}, L_{f_3}$ (or pseudoranges) at three different frequencies in L-band, f_1, f_2, f_3 (see for instance Wang et al. 2005).

Unfortunately, this approach is not feasible when combining observations at close frequencies in L-band, because the difference of the second order differential effect is too small compared with the phase measurement error (thermal noise, multipath and antenna center error), as it is going to be demonstrated theoretically, and checked later on with actual three-frequency data.

I_f	k	$I_f \cdot (-f^k/\alpha_f)$	Considered Approximations	α_f (S.I. units)	$I_c/(-I_f \cdot f^k)$	$I_c(P)/I_c$ $= I_f(P)/I_f$	GNSS prod. main. affected	
First order ($I_{f,1}$)	2	$S = \int_S^R N_e dl$	-	40.309	0	-1	Rec. coord.	up to meters
Second order ($I_{f,2}$)	3	$\int_S^R B \cdot \cos\theta N_e dl$	$B_0 S \cos\theta_0$ $B_0 MV \cos\theta_0$	$1.1284 \cdot 10^{12}$	$\frac{1}{f_1 f_2 (f_1+f_2)}$	-2	Z-sat. coord. Sat. clocks	$< 11mm$ +/- 20 ps
Third order (N_e^2-term, $I_{f,3,M}$)	4	$\int_S^R N_e^2 dl$	$\eta N_m S$ $\eta N_m MV$	812.42	$\frac{1}{f_1^2 f_2^2}$	-3	-	
Third order (B-term, $I_{f,3,s}$)	4	$\int_S^R N_e B^2 (1+\cos^2\theta) dl$	${B_0}^2 S(1+\cos^2\theta_0)$ ${B_0}^2 MV(1+\cos^2\theta_0)$	$1.5793 \cdot 10^{22}$	$\frac{1}{f_1^2 f_2^2}$	-3	-	
Geometric bending ($I_{f,g}$)	4	$\frac{S^2 e^{-\beta E}}{H_{F2} h_{m,F2}^{1/8}}$[*]	$\frac{2.495 \cdot 10^8}{7.5 \cdot 10^{-5}} \left[(1-0.8595\cos^2 E)^{-1/2} - 1\right] S^2$[**] $\frac{2.495 \cdot 10^8}{7.5 \cdot 10^{-5}} \left[(1-0.8595\cos^2 E)^{-1/2} - 1\right] M^2 V^2$	$-7.5 \cdot 10^{-5}$[*]	$\frac{1}{f_1^2 f_2^2}$	1	Z-sat. coord. Sat. clocks	< 3mm -3 to +6 ps
dSTEC bending ($I_{f,d}$)	4	$\int_S^R \frac{a^2}{r^2-a^2} N_e dl$	$\frac{0.1108 \cdot e^{-\gamma E}}{40.309^2 \cdot f^2 \cdot H_{F2} \cdot (h_{m,F2})^{0.3}} S^2$[***] $\frac{0.1108 \cdot e^{-\gamma E}}{40.309^2 \cdot f^2 \cdot H_{F2} \cdot (h_{m,F2})^{0.3}} M^2 V^2$	40.309^2	$\frac{1}{f_1^2 f_2^2}$	-1	Z-sat. coord. Sat. clocks	up to -7 mm -15 to +12 ps

Table 1 The main contents of this table are: Basic dependences of high order ionospheric terms (second, third and fifth column), considered approximations (fourth column), impact on first-order ionospheric-free combination of carrier phases, Lc (sixth column), and of pseudoranges, Pc (seventh column) and main impact on precise GPS products following this work (eighth and nineth columns). Moreover the considered approximations are included in fourth column.

3.1 Theoretical analysis

From Equation 1 and taking into account expressions in Table 1, one can express (by neglecting $I_{f,3}$, $I_{f,g}$ and $I_{f,d}$):

$$\begin{cases} L_1^\star = \rho^\star - \frac{s_1}{f_1^2} - \frac{s_2}{f_1^3} \\ L_2^\star = \rho^\star - \frac{s_1}{f_2^2} - \frac{s_2}{f_2^3} \\ L_3^\star = \rho^\star - \frac{s_1}{f_3^2} - \frac{s_2}{f_3^3} \end{cases} \tag{2}$$

where $L_1^\star, L_2^\star, L_3^\star$ represent the GNSS carrier phases once corrected from the wind-up and ambiguity terms,

$$L_i^\star = L_{f_i} - B_{f_i} - \frac{c}{f_i}\phi \tag{3}$$

$\rho^\star$ is the first and second order ionospheric-free combination of carrier phases, $s_1 = -I_{f_i,1} \cdot f_i^2$ and $s_2 = -I_{f_i,2} \cdot f_i^3$. $i = 1, 2, 3$, are the non-frequency dependencies of the first and second order ionospheric delay, as previously detailed.

From Equation 2, it is straightforward to isolate $\rho^\star$, the first order coefficient s_1 (which can be approximated[1] from $L_1^\star$ and $L_2^\star$ only, by neglecting s_2 in Equation 2) and the second order coefficient s_2:

$$\rho^\star = \frac{L_1^\star \left(\frac{1}{f_2^2 f_3^3} - \frac{1}{f_2^3 f_3^2}\right) + L_2^\star \left(\frac{1}{f_3^2 f_1^3} - \frac{1}{f_3^3 f_1^2}\right) + L_3^\star \left(\frac{1}{f_1^2 f_2^3} - \frac{1}{f_1^3 f_2^2}\right)}{\left(\frac{1}{f_2^2 f_3^3} - \frac{1}{f_2^3 f_3^2}\right) + \left(\frac{1}{f_3^2 f_1^3} - \frac{1}{f_3^3 f_1^2}\right) + \left(\frac{1}{f_1^2 f_2^3} - \frac{1}{f_1^3 f_2^2}\right)} \tag{4}$$

But when a simple[2] estimation of its standard deviation is done, in terms of the standard deviation of $L_1^\star$, $L_2^\star$ and $L_3^\star$ after removing the modelled term ($\sigma_i \simeq 0.01\,\lambda_i \equiv \sigma_L \;\; \forall i = 1, 2, 3$ where $\lambda_i = \frac{c}{f_i}$, being c the speed of light in a vacuum), the following

[1] This very good approximation gives $s_1 \simeq \frac{f_1^2 f_2^2}{f_1^2 - f_2^2}(L_1^\star - L_2^\star)$, with an error less than 1‰

[2] The observational errors are assumed independent and distributed as Gaussian random variables, associated to thermal noise only, hence with values which are proportional (1%) of each given wavelength λ_i (see, for instance, Sanz Subirana et al. 2012).

expression is obtained:

$$\sigma\left[\rho^{\star}\right]=\sigma_{L}\sqrt{\frac{\sigma_{1}^{2}\left(\frac{1}{f_{2}^{2}f_{3}^{3}}-\frac{1}{f_{2}^{3}f_{3}^{2}}\right)^{2}+\sigma_{2}^{2}\left(\frac{1}{f_{3}^{2}f_{1}^{3}}-\frac{1}{f_{3}^{3}f_{1}^{2}}\right)^{2}+\sigma_{3}^{2}\left(\frac{1}{f_{1}^{2}f_{2}^{3}}-\frac{1}{f_{1}^{3}f_{2}^{2}}\right)^{2}}{\left[\left(\frac{1}{f_{2}^{2}f_{3}^{3}}-\frac{1}{f_{2}^{3}f_{3}^{2}}\right)+\left(\frac{1}{f_{3}^{2}f_{1}^{3}}-\frac{1}{f_{3}^{3}f_{1}^{2}}\right)+\left(\frac{1}{f_{1}^{2}f_{2}^{3}}-\frac{1}{f_{1}^{3}f_{2}^{2}}\right)\right]^{2}}} \quad (5)$$

From these expressions, huge error augmentation factors, of one order of magnitude or even more, are found for all available L-band combinations of simultaneous measurements at three GNSS frequencies (see bold values in Table 2 for current or scheduled GNSSs: GPS, GLONASS, Galileo or Beidou). This occurs to the first and (plus) second order ionospheric-free combination $\rho^{\star}$, and for the first and second order terms $-s_1/f^2$ and $-s_2/f^3$. The huge errors especially happen when $\rho^{\star}$ is compared with the almost exact first-order ionospheric-free combination $\tilde{\rho}^{\star}$ (see Table 2). Such augmented noise affects as well to $-s_2/f^3$, at the level of ten centimeters, higher than the highest expected second order ionospheric term, of which the cancellation is an important goal in very precise positioning (see Boehm et al. 2010, page 141, Table 9.2). At this point, it can be concluded that no useful simultaneous first and second order ionospheric delay cancellation is expected from combining three simultaneous measurements of GNSS carrier phases at three L-band frequencies, unless frequencies at different bands (like Ku, C and N1 or N2) are combined (see again Table 2).

This theoretical conclusion has been confirmed with actual measurements. An experiment has been carried out using three-frequency L-band GNSS data confirming the difficulties to isolate/mitigate the 2nd-order ionospheric correction term, in spite of applying carrier phase multipath and antenna phase diagram error mitigation. Details are given in next subsection.

3-freq. GNSS carrier phase comb.	f_1 (GHz)	f_2 (GHz)	f_3 (GHz)	$\sigma[\rho^\star]$ (cm)	$\sigma[\tilde{\rho}^\star]$ (cm)	$\sigma[\frac{-s_2}{f_1^3}]$ (cm)
GPS-L1-L2-L5	1.57542	1.22760	1.17645	**8.3**	0.6	**11.0**
GLONASS-G1-G2-G3	1.60200	1.24600	1.202025	**9.6**	0.6	**12.8**
Galileo-E1-E6-E5a	1.57542	1.27875	1.17645	**5.0**	0.7	**6.6**
Beidou-B1-B2-B3	1.561098	1.20714	1.26852	**8.5**	0.6	**11.8**
Mixed-Ku-C-L1	15.34500	5.11500	1.57542	0.0	0.0	0.0
Mixed-L1-N1-N2	1.57542	0.40000	0.15000	0.2	0.2	0.0
Mixed-Ku-L1-N2	15.34500	1.57542	0.15000	0.0	0.0	0.0
Mixed-Ku-C-N2	15.34500	5.11500	0.15000	0.0	0.0	0.0

Table 2 The expected noise for certain relevant existing (first block) and hypothetical (second block) combinations of carrier phase measurements in three frequencies used in Space Geodesy (1st to 4th columns) is shown. It has been computed under the assumption of gaussian, indepedent carrier phase noise at three frequencies with an standard deviation of 1% for each given wavelength The standard deviations are given for $\rho^\star$ (the 3-frequency combination removing both first and second-order ionospheric delays), $\tilde{\rho}^\star$ (2-frequency first-order ionospheric free combination) and $-\frac{s_2}{f_1^3}$ (the ionospheric second order term at the higher frequency of the combination). It can be seen how the usage of three-frequency L-band measurements for computing either $\rho^\star$ or $-\frac{s_2}{f_1^3}$ increases the noise one order of magnitude (up to several centimeters, typically higher than the higher-order ionospheric dependence) compared with the dual-frequency combination $\rho^\star$.

3.2 Validation using actual three-frequency measurements

Recent modernized GPS data at 1-Hz ($L1$, $L2$ & $L5$) from the low latitude IGS receiver WUH2, at Wuhan (China), have been analyzed during Fall season of year 2011. Local midnight conditions have been selected, with very small electron content, evidencing the augmented errors (multipath, antenna calibration errors and thermal noise) included

in the three carrier-phase combination providing I2$\simeq I_{c,2}$ (with an expected value of almost zero).

When the first and second order ionospheric-free combination is done, involving three simultaneous frequency carrier phase observations in L-band, the measurement error is amplified very significantly (one order of magnitude), due to the close frequencies involved.

The I2 term (plus an ambiguity term) has been first computed (second order ionospheric effect for L_c in the context of this experiment) for every epoch in which the GPS satellite PRN25 has been measured (see Figure 1). This is done for two close available days in 2011: 298 (magenta points) and 296 (blue points), from the combination of the simultaneous phase measurements in three GPS L-band frequencies (L1, L2 and L5). Afterwards the difference of every I2 value for day 298 minus the corresponding value two sidereal days before (also with available data in geomagnetically quiet conditions) is taken, in such a way that the Line-Of-Sight (LOS) are almost the same (the GPS satellite has performed 4 orbits and the Earth two whole rotations, brown points). In this way, the multipath and phase center errors on I2 (strongly LOS dependent) are mitigated very significantly: the deviations fall up to about 10 cm, instead up to about 25 cm. However this remaining signal cannot be considered as an actual second order ionospheric determination, because $I1$, which should be three orders of magnitude larger, is almost zero. Indeed this is clearly seen after performing exactly the same computation but for first order term I1 (deduced from L1 and L2 measurements, red and green points for days 298 and 296, and the two-sidereal-day difference dI1 in dark blue).

In short, it can be seen in Figure 1 that the peaks in $dI2$ are not at all related with the actual $I2$ value, because their variations are much greater than the $I1$ variations

($LI \equiv L_1 - L_2$ curves), instead of about 1000 times smaller as it should be expected. Instead of that, they appear associated with the remaining residual multipath (looking for instance at LI). Moreover, the $dI2$ noise is at the level of a few centimeters, compatible with above described theoretical expectations, confirming the lack of usefulness of the combination of three-frequency simultaneous GNSS carrier phase measurements in L-band, in order to cancel-out the ionospheric second-order term as well.

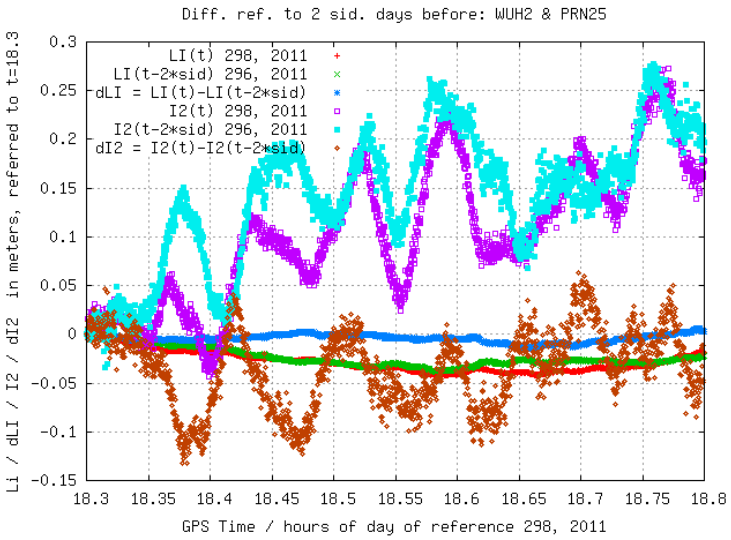

Fig. 1 LI, dLI (sidereal-day difference), $I2$ and $dI2$ (sidereal-day difference) effect comparison for day 298 of year 2011 and, approximately, two sidereal days earlier, i.e. 296, 2011. Data source: actual $L1$, $L2$ and $L5$ GPS carrier phase measurements from the IGS receiver WUH2 and the GPS satellite transmitting PRN25.

4 Assessment of I2+ effects in range

In order to assess the different higher order ionospheric terms, realistic simulations of I2+ terms under Solar Maximum conditions have been performed using their exact

expressions (given in the third column of Table 1). On the one hand, the ISO model "International Reference Ionosphere 2012" (IRI2012) has been used for the ionospheric electron densities, setting the driving parameters (the sunspot number and ionospheric indices, Rz12 and IG12 respectively) to the maximum values recorded so far, during March 1958 ($RZ12 = 201.3$ and $IG12 = 165.6$). On the other hand, the most reliable geomagnetic field source has been also implemented: the "International Geomagnetic Reference Field", IGRF11 (see for instance Matteo and Morton, 2011).

Before adopting the geometry of actual observations from a global worldwide network of permanent GNSS receivers, a grid of virtual receivers (red cloud in Figure 2) and virtual satellites (green points) has been simulated to better understand the range distribution of higher-order ionospheric effects in terms of the LOS user elevation and azimuth. The adopted grid resolution is 10^o x 10^o in longitude and latitude, and elevations at 10^o, 30^o and 60^o, and azimuths at 0^o, 90^o, 180^o and 270^o (North, East, South and West directions, respectively). For instance, Figure 3 presents the distribution of

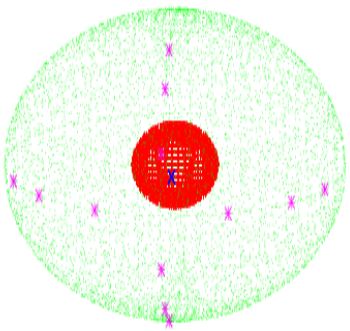

Fig. 2 Grid of virtual receivers (red points) and virtual satellite (green points). The particular virtual satellites (pink crosses) "seen" from an equatorial receiver (blue cross) are also depicted corresponding to the North, South, East, West directions at elevations of 10^o, 30^o and 60^o.

second-order ionospheric effects on L_c combination (I_2) on North, South, East, West directions at low (10^o) and high elevations (90^o). Notice that, at mid North latitudes, the observations of satellites seen towards the South are much more affected, about 50% higher than for the remaining directions. This can be explained by the geometry of the geomagnetic lines (see Figure 4) and the main dependence of I_2 on the magnetic field projection over the propagation direction. Another remarkable point is that I_2 does not vanish at high elevations (see central plot in Figure 3), reaching up to 5 mm at north mid latitudes, in agreement with the projection dependence of I_2.

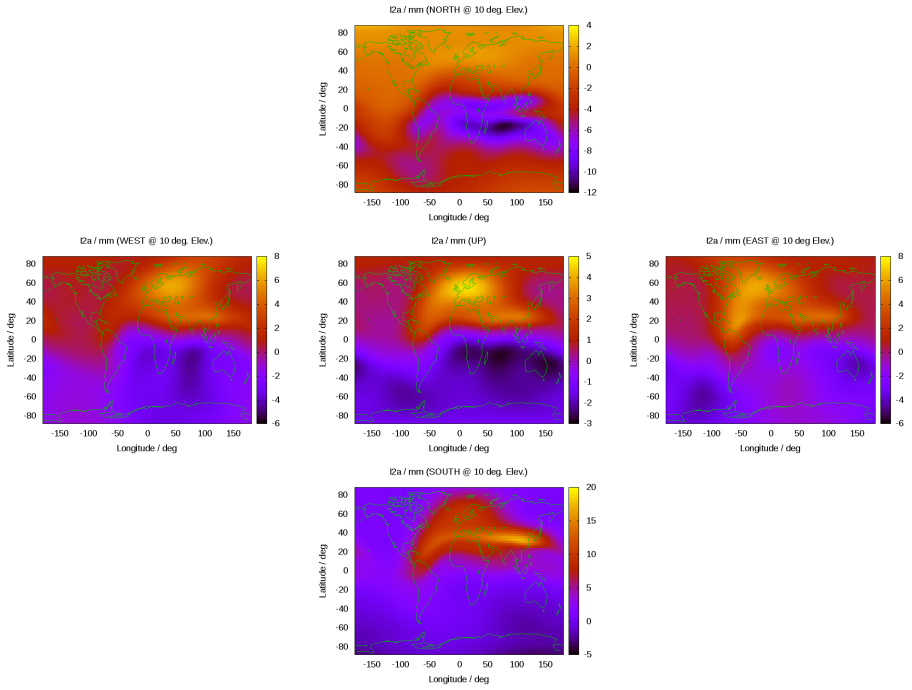

Fig. 3 Worldwide I2 simulated true value in meters (integrating the accurate expression for second-order ionospheric term) for 10 deg. LOS observations at North (top, from -12 to +4 mm), South (bottom, from -5 to +20 mm), East (right, from -6 to +8 mm), West (left, from -6 to +8 mm) and vertical directions (middle, from -3 to +5 mm) obtained from IGRF11 and IRI2012 for the nominal solar maximum conditions adopted in the study, at 12UT.

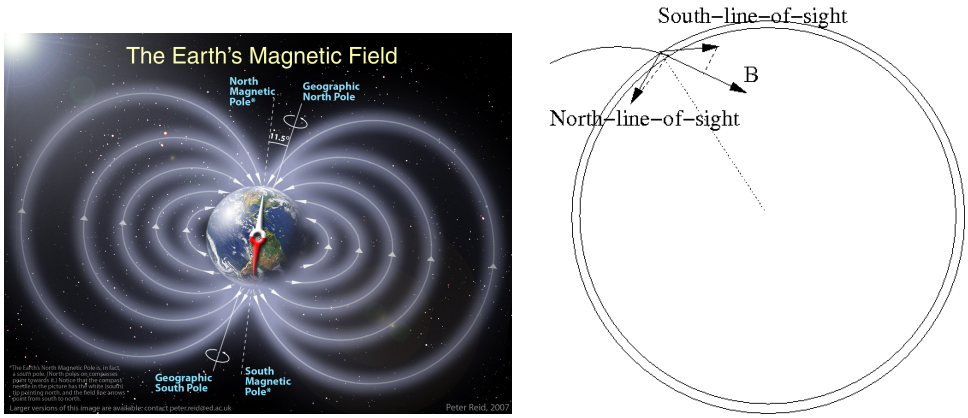

Fig. 4 Left: Representation of the field lines of the geomagnetic field (source: http://www.epa.gov). Right: Main projection components of the geomagnetic field along two low-elevation LOS directions, northward and southward, for a mid-latitude GNSS receiver.

Another remarkable point, which can easily be realized through this simulation with the grid of virtual stations and GNSS receivers, is the comparison of the distribution of the four main higher-order ionospheric terms (second order, third order, geometric bending and differential STEC bending terms, $I_{c,2}$, $I_{c,3}$, $I_{c,g}$ and $I_{c,d}$ respectively, see Table 1). They are computed for the first-order ionospheric-free combination of carrier phases (L_c), used in precise GNSS processing. In Figure 5 the comparison for southward observations at an elevation of 10^o shows that the highest values are attained by the second order and dSTEC bending terms $I_{c,2}$ and $I_{c,d}$ (up to more than 1 cm), The geometric bending effect $I_{c,g}$ reaches up to about half a centimeter, and finally the third order term $I_{c,3}$ remains at the millimeter level. We will show in next section how this higher-order ionospheric terms affect different precise GNSS products. However, for high elevation observations only $I_{c,2}$ (as it has been discussed above) and also $I_{c,3}$ (but at sub-millimeter level) do not vanish, as expected.

Moreover, by activating the IRI2012 STORM module (see Araujo-Pradere et al. 2003), it is possible to have a first glance on the behaviour of higher-order ionospheric terms under storm conditions. The conditions chosen are of a major geomagnetic storm ocurring at around 72000 seconds UT for day 324 of year 2003. The main modelled effects can be seen in Figure 6 consisting of strong E-layer enhancement at high latitudes, causing huge effects specially in the bending terms: $I_{c,g}$ up to 10 cm and $I_{c,d}$ up to 7 cm. Nevertheless, the most important effect is related to the high associated gradients at high latitudes around noon.

Finally we have confirmed as well the consistency of the adopted model in range, comparing in particular the I2 prediction computed with IRI, with those values ob-

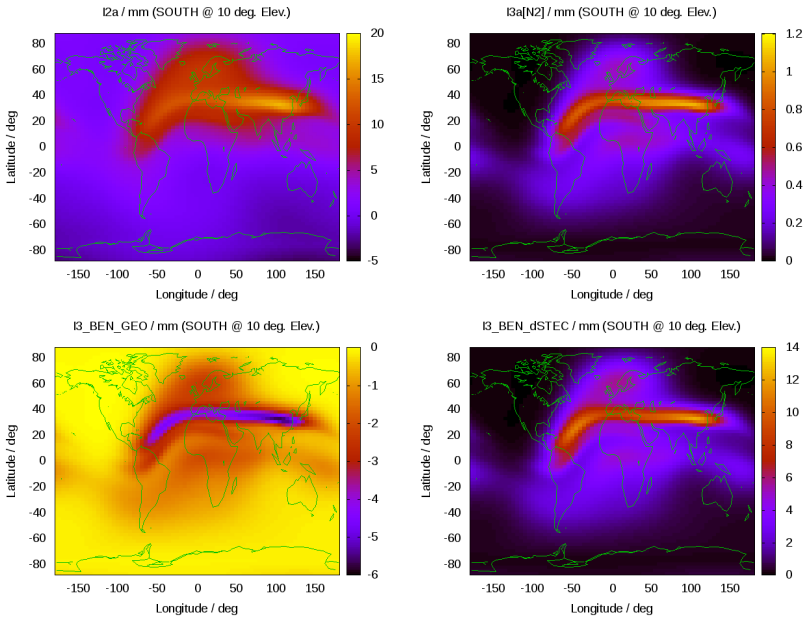

Fig. 5 Higher-order ionospheric terms in L_c carrier phase combination: second and third order terms and the geometric and dSTEC bending components, $I_{c,2}$, $I_{c,3}$, $I_{c,g}$ and $I_{c,d}$, from left to right, from top to bottom, respectively, generated in nominal solar maximum conditions with IRI2012 and IGRF11, for south and 10 deg. elevation line-of-sight.

tained directly from actual receiver data, following the approach of Hernández-Pajares et al. 2007.

5 I2+ impact on global GNSS network solutions

This section will evaluate the impact of the I2+ terms and of their approximated modeling on precise GNSS applications. The different approximations for each I2+ term, which will be compared among them and the considered true value, are the ones previously introduced in Table 1 (column 4 and 3 respectively, taking into account column 5). In particular the magnetic field modulus is extracted out of the corresponding LOS

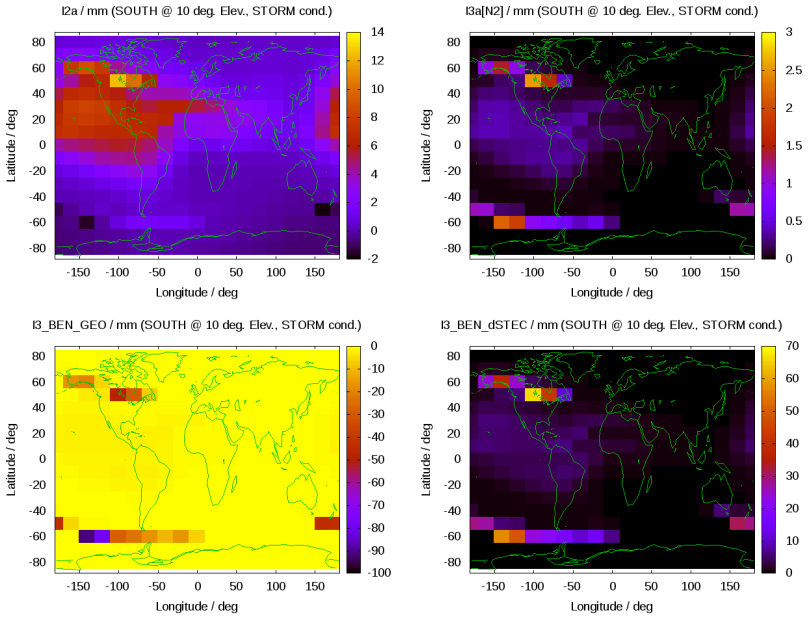

Fig. 6 Higher-order ionospheric terms in L_c carrier phase combination (in meters) generated in storm conditions for epoch 72000 seconds of day 324, year 2003, with IRI2012 and IGRF11, for south and 10 deg. elevation LOS. From left to right, from top to bottom: Second and third order terms and the geometric and dSTEC bending components, $I_{c,2}$, $I_{c,3}$, $I_{c,g}$ and $I_{c,d}$, respectively (similarly to the previous plot).

integrals (for one of the third order terms, among the second order one). The squared electron density integral is expressed in terms of the electron density peak by means of the Chapman model (main third order term). Heuristic approximations for both geometric and differential STEC bending effects are used as well. Among that the approximation of STEC in terms of VTEC and the mapping function (assuming an effective ionospheric height of 450 km) has been considered as well in all the terms.

To evaluate the impact of I2+ terms and approximated corrections on precise products and applications, a worldwide selection of 44 actual IGS stations has been used under the actual GPS constellation (see Figure 7). The impact was computed inde-

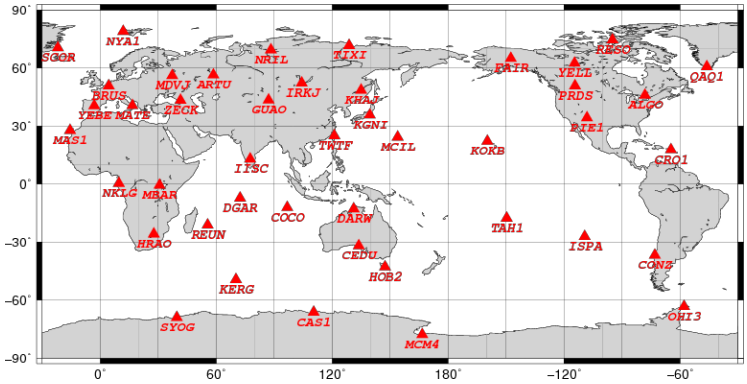

Fig. 7 Worldwide distributed subset of selected IGS receivers used in this study.

pendently by means of two renowned geodetic software tools: GIPSY-OASIS2 (GOA) (Zumberge et al. 1997) and BERNESE (Dach et al. 2007). By intercomparisons, the consistency of the results was perfectly verified. For the sake of clarity, only the results obtained with GIPSY will be shown in this section.

GPS observations in RINEX format corresponding to the global network and actual GPS constellation were simulated for one representative day (day 060 of year 2009) but assuming Solar Maximum conditions. The higher-order terms computed with IRI2012

and IGRF2011 were then added to the pseudorange and carrier phase simulated data. The set of RINEX data so-obtained has been processed afterwards in a non-fiducial zero-differenced approach. This latter is indeed better suited to obtain very accurate results (see for instance Rius et al 1995). The main products in the global network solution have been analyzed such for the receivers (3D position, non-hydrostatic zenith tropospheric delay, receiver clock bias) and for the GPS satellites (orbits, satellite clock biases). The impact is assessed by comparing the results with the range including each given higher-order term or mitigation error, with (minus) the results from the observations with no higher order ionospheric error. In addition, we also determined the remaining errors when the I2+ terms are corrected with simplified models. To do so, we differentiated the results obtained from data with the accurate I2+ added and the simplified modeled I2+ removed, with the results obtained from data without any I2+ effect.

5.1 Assessing the I2 impact

In order to confirm the consistency of the approach adopted in this research, we first look at the impact of second order term which can be directly compared with the results obtained in previous works performed with actual data, such as Hernández-Pajares et al. 2007. Figure 8 shows the impact of the second-order ionospheric term, $I_{c,2}$ under nominal solar maximum conditions in range (daily average per receiver), carrier phase ambiguity (phase bias), static positioning and clock error.

The most remarkable results confirm the consistency of the overall approach: firstly look at the carrier phase ambiguity (phase bias). It is, in general, a nuisance parameter, but its computation becomes a reliable first-glance test to check the consistency of the

results. Indeed, as it is shown in Hernández-Pajares et al. 2007, the phase bias should be correlated with I2, as expected from the relationship $Bc = Lc - Pc$ from which it can be deduced that $Bc \approx 3 \cdot I2$ (see third row and seventh column in Table 1). Such effect of I2 on the Lc phase ambiguity (top-right plot versus top-left plot in Figure 8) is confirmed by the results (about 3 times I2).

The I2 impact on receiver position (a main target in GNSS) is also consistent (second row-left hand plot of Figure 8). The Up component appears anticorrelated with I2 (top-left), as expected. And a relatively small effect (up to few mm) is found, as reported in Hernández-Pajares et al. 2007, analyzing actual data.

The second order ionospheric term effect on station clock error (bias), which directly impacts on GNSS applications for precise time transfer, reaches up to $\approx$ 5mm (or 15 picoseconds), and is anticorrelated with I2, which is compatible with a main I2 effect on the receiver clock (taking into acccount in Equation 11 of Hernández-Pajares et al. 2007 that Pc is affected by a $-2 \cdot I2$ factor).

With respect to the non-hydrostatic zenith tropospheric delay (a key term for GNSS weather forecasting applications), the I2 effect is very small, approximately between 0.1 up to 0.2 mm, compatible with the different elevation dependences of I2 and the tropospheric delay, respectively. Indeed, literature does not cite it as significantly I2-affected.

Other important products in global network GNSS processing are the precise satellite orbits. The average error in the geocentric coordinates of GPS satellites also reflects the impact on the geocenter estimation. A positive bias of about 5 mm was found on the Z-component of GPS satellites (bottom-left plot in Figure 8), compatible with the main "dipolar" geocenter signature distribution of I2, positive to the North, obtained in Hernández-Pajares et al, 2007.

Finally, the mean effect on satellite clocks (which is averaged directly in range) is quite small (see bottom-right plot in Figure 8), but the individual values can reach up to close to 1 cm (or 30 ps), like in the above mentioned paper.

5.2 Impact of all higher order ionospheric terms

Table 3 presents a summary of the range of values achieved for every I2+ term, for the range itself (at elevations of 10^o and 90^o) and for the estimated geodetic parameters. In each case the effect of the I2+ term is provided, and the impact of the modeling errors when simpliefied mitigation strategies are used (as described in Table 1). All the results correspond to Solar Maximum geomagnetically quiet conditions (the maximum TEC value ever observed, but under normal geomagnetic conditions) the independent runs performed with GIPSY and BERNESE softwares, gave consistent results as shown for example in Figure 9, which presents the comparisons of higher order ionospheric impact on satellite clocks estimated by means of GIPSY and BERNESE. For the sake of clarity, only the results with GIPSY runs are included for the global network solutions in Table 3. The values above 1 mm / 3 ps are indicated in red, and the most remarkable (greater than 5 mm / 15 ps) are enhanced in bold font.

From the analysis of the results, it can be concluded that the major impact of the I2+ perturbations comes from the I2 term as expected. It has the highest magnitude at low elevation where it can reach, in this case of Solar Maximum geomagnetically quiet conditions, up to 2 cm on the range. The I2 impact on the range induces a geocenter artificial displacement of 4 mm, more than 1 cm error on the satellite orbits, and up to almost 30 ps on the satellite clocks. The tropospheric zenith delay is not affected by

Term	Range val. @ $ele = 10^o$ (mm)	Range val. @ $ele = 90^o$ (mm)	Z-Sat. Coor. GIPSY (mm)	Sat. clocks GIPSY (ps)	Rec. pos. GIPSY (mm)	Rec. clocks GIPSY (ps)	ZTD GIPSY (mm)
I2	**-12 to 20**	-3 to 5	**-2 to 11**	**-22 to 28**	-1.8 to 2	-12 to 15	-0.3 to 0.5
I2 corr. (VTEC)	-5 to 2	-0.5 to 0.4					
I2 corr. (STEC)	-1.6 to 0.4	-0.3 to 0.3	-1 to 1	-3 to 2	-0.3 to 0.2	-3 to 2	-0.1 to 0.1
I3	0 to 1.2	0 to 0.4	-1 to 0.5	-1 to 1	-0.2 to 0.2	-2 to 0.1	0 to 0.1
I3 corr. (VTEC)	-0.3 to 0.2	-0.1 to 0	-0.1 to 0.1	-0.1 to 0.1	-0.1 to 0.2	-0.1 to 0.1	0.0
I3 corr. (STEC)	-0.1 to 0.0	-0.1 to 0					
Geo-bend.	-6 to 0	0.0	0.1 to 3	-3 to 6	-0.5 to 0.5	-1 to 4	-0.6 to 0
Geo-bend. corr. (VTEC)	-1.5 to 3	0.0	-2 to 0.5	-2 to 3	-0.2 to 0.2	-2 to 0.0	0 to 0.4
dSTEC-bend.	**0 to 14**	0	-7 to 0	-15 to 12	-1 to 1	-11 to 4	-0.2 to 1.4
dSTEC-bend. corr.	**-1 to 2**	-0.1 to 0	-2 to 0	-3 to 2	-0.4 to 0.4	-2 to 0.1	-0.1 to 0.3
All			-5 to 8	**-31 to 32**	-1.6 to 2.6	-14 to 14	-0.2 to 1.1
All corrected			-4 to 1 (61%)	-7 to 5 (80%)	-0.4 to 0.3 (83%)	-4 to 1 (82%)	-0.1 to 0.7 (38%)

Table 3 Some key numbers summarizing the impact of I2+ terms and the remaining effect when they are corrected using a simplified modeling: 2nd and 3rd columns are in the range domain (full range of values for 10^o and 90^o of elevation respectively), and the other columns contain the effect on estimated parameters with GIPSY (equivalent results are obtained with BERNESE) in global network processing with the actual geometry of Figure 7 (range defined by bias -/+ standard deviation; from 4th column). ZTD stands for non-hydrostatic Zenith Tropospheric Delay. The Solar Maximum conditions are recreated with the IRI2012, for the maximum values of the two main driven parameters since 1958 (Rz12 = 201.3 and IG12=165.6). Color code: values above 1 mm (above 3 ps in time) appear in red, and the most remarkable ones, greater than 5 mm (15 ps in time), are in bold font. Finally the last row includes in parenthesis as well the percentage of error reduction with the proposed modeling, in each geodetic parameter estimated in the global GPS network solution.

the I2 term, thanks to the very high elevation-dependence of the tropospheric delay, while I2 has only a factor 4 between high and low elevation values.

The second-most important impact by order of magnitude is the dSTEC bending, i.e. the impact on the dual-frequency ionosphere-free combination Lc caused by the difference in STEC of the signals with different frequencies due to their different bending (and hence path) while crossing the ionosphere. This term is very large at low elevation (up to 1.4 cm on the range), but decreases down to zero at the zenith. Its impact on the geodetic parameters is not negligible. It reaches the level of 7 mm on the satellite orbits, and 15 ps on the satellite clocks. It must be noted that for the tropospheric delay, the dSTEC bending has a larger impact than the I2 term (up to more than 1 mm).

The geometric bending has a lower impact than the dSTEC bending, but with the opposite sign (see Table 1). Correcting for this term without a correction of the dSTEC bending should not be recommended as it would reinforce the effect of the dSTEC bending, as this latter is partly mitigated by the effect of geometric bending on the range.

Table 3 also shows for each I2+ term the remaining error when it is corrected (or mitigated) using a simple and feasible modeling. Finally the global impact of the I2+ terms, as well as the global remaining error after mitigation is presented (last row in Table 3), including the percentage of error reduction. The I2+ errors are shown to be mitigated at the level of 60-80% for the most affected geodetic parameters (Z-coordinate of GPS satellites, satellite clocks, receiver positions and receiver clocks). From these results, we also recommend to use the correction using the observed STEC, deduced from the geometry-free combination, which is in all cases (I2, I3, geometric

bending and dSTEC bending) better than when using an external VTEC product for a given height, combined with a mapping function.

Finally the impact of the I2+ terms on PPP solutions was estimated, using the ATOMIUM software (Defraigne et al, 2008). PPP was computed for 44 receivers of the study (Figure 7), in a consistent way, i.e. using the GNSS precise products computed with BERNESE and the same I2+ modeling. As an example, Figure 10 shows the remaining impact on the receiver clock solutions when the complete I2+ is present in the observations and satellite products, and when the complete I2+ was corrected with simplified models.

We can observe that even if the satellite orbits and clocks have absorbed the major part of I2+ delays, there is a remaining effect on the PPP clock solution at the level of 10 ps when the noise of the solution is ignored. However, when I2+ terms are corrected with simplified models, then the remaining errors on the PPP solution (reduced up to more than 60%) are lower than the noise level.

6 Conclusions and recommendations

A deep analysis of I2+ values and mitigation error impact on GNSS precise networks and user solutions has been performed with actual geometry and realistic simulated values under high Solar Maximum conditions. Concerning the possibility to work with three frequencies, there are strong observational evidences that the L-band three-frequency combination cancelling the first and second order ionospheric delays is not suitable for high precise GNSS applications due to the huge increase (more than 20 times) of measurement errors (such as thermal noise error, multipath and unmodelled antenna phase center errors). Consequently, the modeling approach is the only one

considered as feasible and useful for I2+ correction/mitigation with L-band GNSS measurements, and the one followed in this work. We calculated accurately the I2+ terms in Lc and Pc for up to 44 worldwide IGS receivers with actual geometry and values corresponding to Solar Maximum conditions simulated with IRI for electron densities, and IGRF11 for the magnetic field. These different I2+ terms have been added to simulated Lc and Pc observations. In parallel, also the remaining errors when correcting the accurate I2+ effect with a simplified and practical modeling have been computed and their difference with respect to the accurate I2+ terms has been added to the simulated Lc and Pc observations. A GNSS precise network solution has then been computed with GIPSY and BERNESE in a non-fiducial approach on all the datasets.

Finally, for each given I2+ term and modeling error, the corresponding impact has been assessed by subtracting the estimated solution from the nominal solution with the raw simulated data. The particular analysis of I2 (the most studied I2+ term), has been performed confirming the consistency of these results with the I2+ distribution in the range domain and compliant with previous studies in the geodetic domain, performed with actual data. The I2 impact represents indeed most of the overall I2+ effect when modeling all the higher order ionospheric terms (more than 80%), being the predominant source of mismodeling in GNSS network solution except for the tropospheric estimation (which is mostly due to both the geometric and dSTEC bending influence). The most remarkable results, after a thorough comparative analysis of the different unmodelled I2+ terms impacting on a GPS network solution, have led to some final recommendations concerning the most noticeable model errors:

– Correcting I2 with the integral approximation expression using direct STEC observations (ionospheric dual-frequency GNSS geometry-free phase measurements after

estimating the ambiguities) reduces the residual error versus the integral approximation expression and deprojected VTEC:

  - The range error, when direct STEC values are used instead of deprojected VTEC, is reduced by a half;
  - The error in receiver coordinates is reduced more than 50% (0.4 mm), similarly to satellite and receiver clocks (less than 1 mm);
  - The estimated troposphere is improved more than 50% (error much less than 0.1 mm) and,
  - The Z-translation derived from the satellite orbits is also reduced by half (up to -0.5 mm).

  In consequence, the correction of $I2$ with the integral expression is good enough, especially if the direct STEC determination is used, in front of STEC derived from deprojected VTEC.

- In case it is not possible to correct both bending effects (geometric and dSTEC), it has been confirmed that it is better not to correct any than just one.
- Results support the IERS recommendation by either aligning along the whole continuous arc of data with the ionospheric combination of dual-frequency pseudoranges (ionospheric-combination pseudorange smoothing with ionospheric-combination carrier phases), or aligning with the STEC computed with global maps (see Hernández-Pajares et al. 2011); or, alternatively, by using the Melbourne-Wübbenna and ionospheric-free ambiguity, estimated accurately from the precise receiver and satellite positions (see Hernández-Pajares et al. 2000).

7 Acknowledgments

The work reported in this paper has been supported under a contract of the European Space Agency (IONO-DeCo) in the frame of the European GNSS Evolutions Programme. The views presented in the paper represent solely the opinion of the authors and should be considered as R&D results not necessarily impacting the present EGNOS and Galileo system design.

8 References

- Araujo-Pradere, E. A., T. J. Fuller-Rowell, and D. Bilitza, Validation of the STORM response in IRI2000, J. Geophys. Res., 108(A3), 1120, doi:10.1029/2002JA009720, 2003.
- Bassiri, S., and G. Hajj, High-order ionospheric effects on the global positioning system observables and means of modeling them, Manuscr. Geod., 18, 280– 289, 1993.
- Bilitza, D., L.-A. McKinnell, B. Reinisch, and T. Fuller-Rowell, The International Reference Ionosphere (IRI) today and in the future, J. Geodesy, 85:909-920, DOI 10.1007/s00190-010-0427-x, 2011.
- Boehm, M., Hernández-Pajares, U. Hugentobler, G. Hulley, F. Mercier, A. Niell, and E. Pavlis, "Chapter 9: Models for atmospheric propagation delays" in IERS Conventions (2010), Gérard Petit and Brian Luzum (eds.), IERS Technical Note No. 36, ISSN: 1019-4568, Verlag des Bundesamts für Kartographie und Geodäie, Frankfurt am Main, 2010.
- Brunner, F., M. Gu, An improved model for the dual frequency ionospheric correction of GPS observations, Manuscr. Geod., 16, 205– 214, 1991.
- Dach, R., U. Hugentobler, P. Fridez, & M. Meindl, Bernese GPS Software Version 5.0, 612p. Astronomical Institute, University of Bern, Bern, Switzerland, 2007.
- Defraigne, P., Guyernon N., and Biuyninx C., GPS time and frequency transfer: PPP and phase-only analysis, Int. Journal of Navig. and Obs., ID 175468, 7 pages, Doi: 10.1155/2008/175468, 2008.
- Hernández, M.; Juan, J.; Sanz, J.; Colombo, O.Application of ionospheric tomography to real-time GPS carrier-phase ambiguities resolution, at scales of 400-1000 km and with

high geomagnetic activity.Geophysical research letters.27 - 13,pp. 2009 - 2012.06/2000 .ISSN 0094-8276, 2000.

- Hernández-Pajares, M., J.M.Juan, J.Sanz and R.Orús, Second-order ionospheric term in GPS: Implementation and impact on geodetic estimates, Journal Geophys. Res., Vol. 112, B08417, doi:10.1029/2006JB004707, 2007.
- Hernández-Pajares, M., J. Miguel Juan, Jaume Sanz, Àngela Aragón-Àngel, Alberto García-Rigo, Dagoberto Salazar, Miquel Escudero, The ionosphere: effects, GPS modeling and the benefits for space geodetic techniques, Journal of Geodesy, December 2011, Volume 85, Issue 12, pp 887-907, 2011.
- Hoque, M. M., and N. Jakowski, Estimate of higher order ionospheric errors in GNSS positioning, Radio Sci., 43, RS5008, doi:10.1029/2007RS003817, 2008.
- Jakowski N., F. Porsch, and G. Mayer, Ionosphere - Induced -Ray-Path Bending Effects in Precision Satellite Positioning Systems, SPN 1/94, 6-13, 1994.
- Kedar, S., G. A. Hajj, B. D. Wilson, and M. B. Heflin, The effect of the second order GPS ionospheric correction on receiver positions, Geophys. Res. Lett., 30(16), 1829, doi:10.1029/2003GL017639, 2003.
- King, M.A., Z. Altamimi, J. Boehm, M. Bos, R. Dach, P. Elosegui, F. Fund, M. Hernández-Pajares, D. Lavallee, P.J. Mendes Cerveira, N. Penna, R. E. M. Riva, P. Steigenberger, T. van Dam, L. Vittuari, S. Williams, and P. Willis, Improved Constraints on Models of Glacial Isostatic Adjustment: A Review of the Contribution of Ground-Based Geodetic Observations, Surv. Geophys., Vol. 31, pp. 465-507, DOI 10.1007/s10712-010-9100-4, 2010.
- Matteo, N.A. and Y.T. Morton, Ionospheric geomagnetic field: Comparison of IGRF model prediction and satellite measurements 1991-2010, Radio Sci., 46, RS4003, doi:10.1029/2010RS004529, 2011.
- Rius, A., Juan, J. M., Hernandez-Pajares, M., Madrigal, A. M., Measuring geocentric radial coordinates with a non-fiducial gps network, Bulletin Geodesique, 69, pp. 320-328, 1995.
- Sanz Subirana, J., J.M. Juan Zornoza, M. Hernandez-Pajares, GNSS Data Processing" (Vol. 1 and Vol. 2), ESA TM-23, ISBN:978-92-9221-885-0 (two volumes), ESA Communications. ESTEC, Noordwijk, the Netherlands, Dec. 2012.

– Wang, Zemin, Yue Wu, Kefei Zhang, Yang Meng, Triple-Frequency Method for High-Order Ionospheric Refractive Error Modelling in GPS Modernization, Journal of Global Positioning Systems, Vol. 4, No. 1-2:291-295, 2005.

– Zumberge, J. F., M. B. Heflin, D. C. Jefferson, M. M. Watkins, F. H. Webb, Precise point positioning for the efficient and robust analysis of GPS data from large networks, J. Geophys. Res., 102 (B3), 5005-5017, doi:10.1029/96JB03860, 1997.

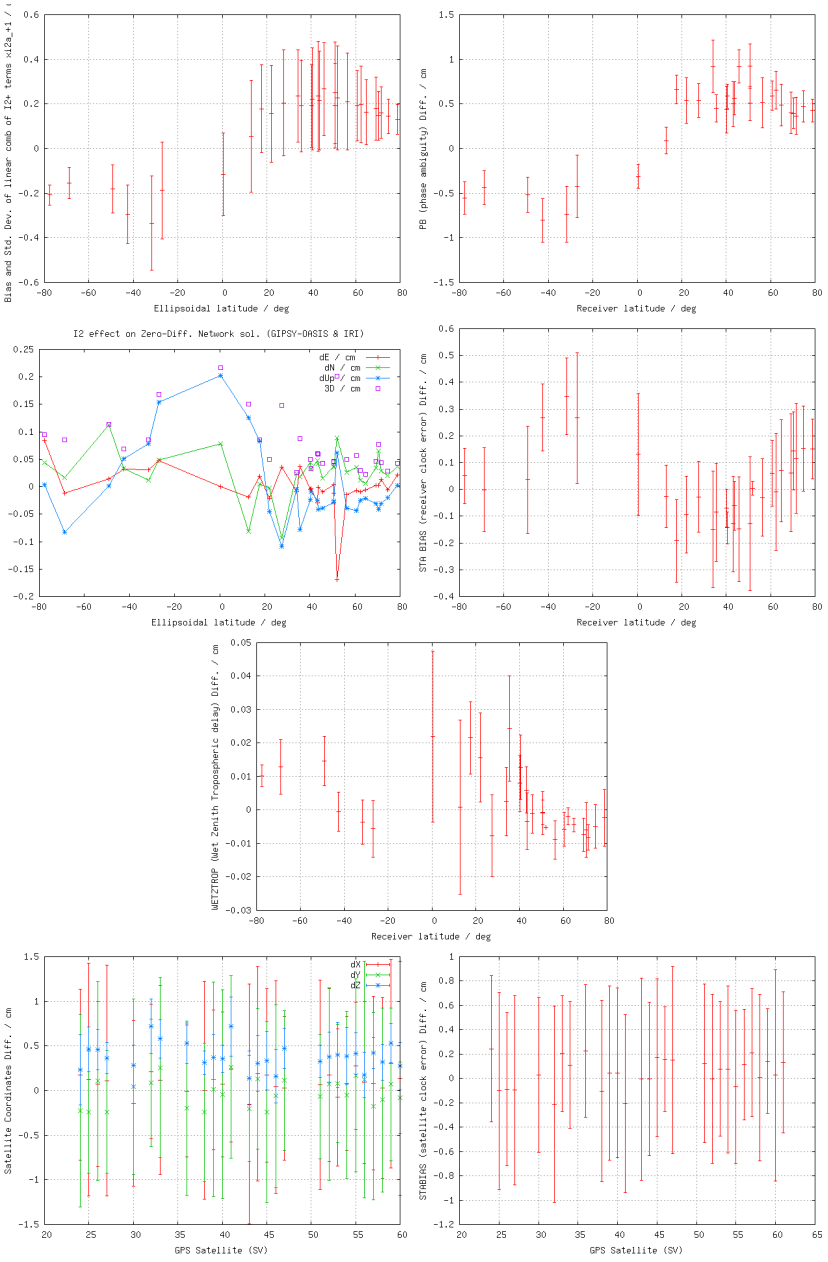

Fig. 8 Second-order ionospheric term effect (in centimeters) on precise geodetic parameters (global network solution) computed with GIPSY. From left to right and top to bottom: Daily average of bias and standard deviation of the impact in range per receiver, carrier phase ambiguity (phase bias), static positioning (error in East-North-Up) clock error and zenith tropospheric delay. Moreover, in function of GPS satellite Space Vehicle number (SV), the bias and standard deviation of satellite orbits and clocks are shown as well, in bottom-left and -right plots, respectively.

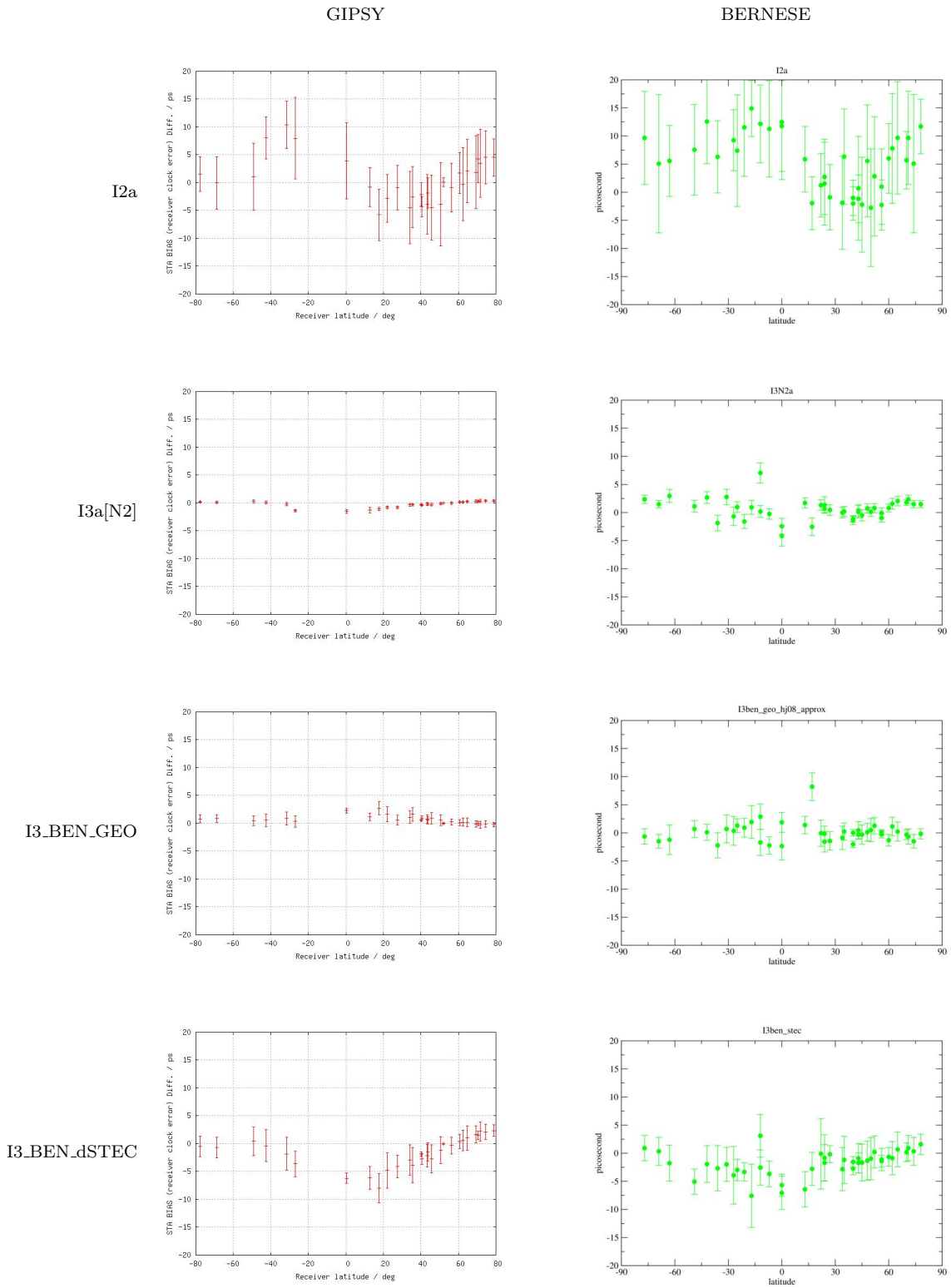

Fig. 9 Comparison of the higher order impact on receiver clock estimation (in ps) between GIPSY (left column) and BERNESE (right column) softwares, for second order term (first row), third order term (second row), geometric and dSTEC bendings (third and fourth rows, respectively).

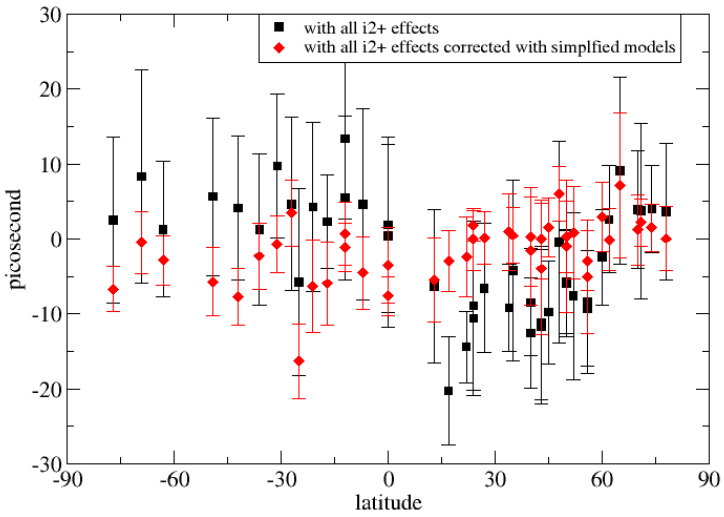

Fig. 10 Daily average receiver clock bias (in picoseconds) versus the latitude of the 44 receivers processed consistently with PPP: Black signs corresponds to no I2+ mitigation and red symbols to I2+ mitigated observations (each point represents the error bias; each error bar the standard deviation).